

Insights into brain architectures from the homological scaffolds of functional connectivity networks

Original

Insights into brain architectures from the homological scaffolds of functional connectivity networks / Lord, L; Expert, P; Fernandes, Hm; Petri, G; Van_harteveld, Tj; Vaccarino, Francesco; Deco, G; Turkheimer, F; Kringelbach, Ml. - In: FRONTIERS IN SYSTEMS NEUROSCIENCE. - ISSN 1662-5137. - ELETTRONICO. - 10:(2016).
[10.3389/fnsys.2016.00085]

Availability:

This version is available at: 11583/2653636 since: 2017-05-22T21:56:29Z

Publisher:

frontiers

Published

DOI:10.3389/fnsys.2016.00085

Terms of use:

This article is made available under terms and conditions as specified in the corresponding bibliographic description in the repository

Publisher copyright

(Article begins on next page)

Insights into brain architectures from the homological scaffolds of functional connectivity networks

Louis-David Lord^{1*}, Paul Expert², Henrique M. Fernandes^{1,3}, Giovanni Petri⁴, Tim J. Van Hartevelt^{1,3}, Francesco Vaccarino^{4,7}, Gustavo Deco^{5,6}, Federico Turkheimer², Morten L. Kringelbach^{1,3}

¹Department of Psychiatry, University of Oxford, United Kingdom, ²Institute of Psychiatry, King's College London, United Kingdom, ³Center of Functionally Integrative Neuroscience, Aarhus University, Denmark, ⁴ISI Foundation, Italy, ⁵Center for Brain and Cognition, Universitat Pompeu Fabra, Spain, ⁶Instituci Catalana de la Recerca i Estudis Avanats (ICREA), Universitat Pompeu Fabra, Spain, ⁷Dipartimento di Scienze Matematiche, Politecnico di Torino, Italy

Submitted to Journal:
Frontiers in Systems Neuroscience

ISSN:
1662-5137

Article type:
Original Research Article

Received on:
11 Jul 2016

Accepted on:
20 Oct 2016

Provisional PDF published on:
20 Oct 2016

Frontiers website link:
www.frontiersin.org

Citation:
Lord L, Expert P, Fernandes HM, Petri G, Van_hartevelt TJ, Vaccarino F, Deco G, Turkheimer F and Kringelbach ML(2016) Insights into brain architectures from the homological scaffolds of functional connectivity networks. *Front. Syst. Neurosci.* 10:85. doi:10.3389/fnsys.2016.00085

Copyright statement:
© 2016 Lord, Expert, Fernandes, Petri, Van_hartevelt, Vaccarino, Deco, Turkheimer and Kringelbach. This is an open-access article distributed under the terms of the [Creative Commons Attribution License \(CC BY\)](https://creativecommons.org/licenses/by/4.0/). The use, distribution and reproduction in other forums is permitted, provided the original author(s) or licensor are credited and that the original publication in this journal is cited, in accordance with accepted academic practice. No use, distribution or reproduction is permitted which does not comply with these terms.

This Provisional PDF corresponds to the article as it appeared upon acceptance, after peer-review. Fully formatted PDF and full text (HTML) versions will be made available soon.

Provisional

Insights into brain architectures from the homological scaffolds of functional connectivity networks

Lord, L.D.¹, Expert, P.², Fernandes, H.M.^{1,3}, Petri, G.⁴, Van Hartevelt, T.J.^{1,3}, Vaccarino, F.⁵, Deco, G.^{6,7}, Turkheimer, F.E.², Kringelbach, M.L.^{1,3}

¹ Department of Psychiatry, University of Oxford, United Kingdom

² Institute of Psychiatry, Kings College London, United Kingdom

³ Center of Functionally Integrative Neuroscience, Aarhus University, Denmark

⁴ Institute for Scientific Interchange (ISI Foundation), Torino, Italy

⁵ Department of Mathematical Sciences, Politecnico di Torino, Torino, Italy

⁶ Center for Brain and Cognition, Universitat Pompeu Fabra, Barcelona, Spain

⁷ Instituci Catalana de la Recerca i Estudis Avanats (ICREA), Universitat Pompeu Fabra, Spain

Correspondence*:

Prof. Morten L Kringelbach

Hedonia Research Group

Department of Psychiatry, University of Oxford,

morten.kringelbach@queens.ox.ac.uk

2 ABSTRACT

3 In recent years, the application of network analysis to neuroimaging data has provided useful
4 insights about the brain's functional and structural organization in both health and disease. This
5 has proven a significant paradigm shift from the study of individual brain regions in isolation.
6 Graph-based models of the brain consist of vertices, which represent distinct brain areas,
7 and edges which encode the presence (or absence) of a structural or functional relationship
8 between each pair of vertices. By definition, any graph metric will be defined upon this dyadic
9 representation of the brain activity. It is however unclear to what extent these dyadic relationships
10 can capture the brain's complex functional architecture and the encoding of information in
11 distributed networks. Moreover, because network representations of global brain activity are
12 derived from measures that have a continuous response (i.e. interregional BOLD signals), it is
13 methodologically complex to characterize the architecture of functional networks using traditional
14 graph-based approaches. In the present study, we investigate the relationship between standard
15 network metrics computed from dyadic interactions in a functional network, and a metric defined
16 on the *persistence homological scaffold* of the network, which is a summary of the persistent
17 homology structure of resting-state fMRI data. The persistence homological scaffold is a summary
18 network that differs in important ways from the standard network representations of functional
19 neuroimaging data: i) it is constructed using the information from all edge weights comprised
20 in the original network without applying an *ad hoc* threshold and ii) as a summary of persistent
21 homology, it considers the contributions of simplicial structures to the network organization rather
22 than dyadic edge-vertices interactions. We investigated the information domain captured by the

23 persistence homological scaffold by computing the strength of each node in the scaffold and
24 comparing it to local graph metrics traditionally employed in neuroimaging studies. We conclude
25 that the persistence scaffold enables the identification of network elements that may support the
26 functional integration of information across distributed brain networks.

27

28 **Keywords:** functional connectivity, fMRI, persistent homology, homological scaffold, integration & segregation

1 INTRODUCTION

29 The application of graph theoretical analysis to neuroimaging data has provided important new insights
30 about the functional organization of the human brain in health and disease. Graph measures considering
31 the global properties of brain networks have notably helped shape our understanding of the system-wide
32 functional architectures which enable the brain to balance the segregation and integration of information
33 in macro-scale networks [6, 7]. Complementary to these system-wide characteristics, local graph metrics
34 have been used to quantify the relative importance of individual brain areas towards routing information in
35 brain networks according to different criteria (section 2.3).

36 Whilst standard graph metrics are powerful descriptive means to characterize functional neuroimaging
37 data at the whole-brain scale, they also involve significant conceptual and methodological limitations.
38 First, these measures are exclusively based on *dyadic* (i.e. pairwise) interactions between edges and
39 vertices. In practice, this means that the basic "unit" of the graph is an edge connecting a pair of nodes. By
40 contrast, it is well established that neural computations performed by distributed ensembles of brain regions
41 underlie higher cognitive phenomena and even resting-state dynamics in the human brain. As described
42 in detail below, methods from *algebraic topology* provide an alternative for encoding such non-dyadic
43 relationships. Specifically, the concept of *simplicial complexes* allows one to describe relations between
44 distributed subpopulations of network elements without sacrificing access to many of the fundamental tools
45 of network science [19].

46 Secondly, the adjacency matrices which form the basis for constructing network representations are
47 derived from measures that have a continuous response and are therefore typically weighted, fully connected,
48 and signed. That is, the value of the pair-wise measure of association (i.e. bivariate/partial correlation,
49 phase synchrony, transfer entropy, mutual information) between the activity signals across brain areas
50 is non-zero, varies considerably across region pairs, and may include both positive and negative values.
51 Therefore, *ad hoc* thresholding methods are commonly employed in functional neuroimaging studies to
52 selectively prune connections within the graph leading to sparser, binary network representations with
53 more naturally interpretable attributes. An exhaustive discussion of the methods used for thresholding
54 brain networks is beyond the scope of this study. It should however be noted that a majority of these
55 strategies lead to the elimination of *weak and/or negative* connections within a network. Yet, it has been
56 demonstrated that standard graph measures are unstable across the threshold ranges typically employed in
57 functional connectivity studies [18] and very few neuroimaging analysis methods actually account for the
58 statistical significance of individual connections [24, 23, 30]. Thus, while neglecting weak links enhances
59 information clarity, it may well do so at the expense of information completeness. Previous studies have
60 indeed shown weak links to significantly contribute to brain functional processes including: resting-state
61 networks, disease states, and cognition [36, 2, 11, 35]. Furthermore, synchronous neural oscillations can be
62 maintained even with very weak synaptic links [8] and complex systems research has provided considerable

63 evidence for the contributions of weak links to the stability of large networks in a range of social and
64 biological systems [20, 12, 29, 28, 27].

65 An alternative to traditional network analysis methods is the use of the *homological scaffolds* of the
66 weighted network [31] to summarise information about the persistent homology of the data. Persistent
67 homology is a recent technique in computational topology [44, 10, 26] that will be described in detail in
68 section 2.2. In summary, homology characterizes a topological space by counting its holes of different
69 dimensions (see 2.2.2 for definitions). Persistent homology characterises the importance and stability
70 of the holes in the original data through a process called filtration. It is accordingly a specific type of
71 *mesoscopic organization* of the vertices and edges and their respective importance that is considered in the
72 persistent homology analysis. This enables one to explore the network's organization from a non-dyadic
73 perspective, consistent with the brain's large-scale ensemble coding mechanisms. Holes are the mesoscopic
74 (anti-)structures remaining in the topological space that are not bounding a higher dimensional simplex.
75 The case of 1-dimensional holes, or "cycles", to which we restrict ourselves in this study, is intuitive to
76 visualise (Fig. 1): a cycle is a closed loop of length greater than three.

77 The network organization of the human brain is characterized by a large number of distributed network
78 modules which perform segregated local computations [33, 38]. There has recently been much interest
79 towards identifying the "hub" regions which enable global communication across segregated brain modules,
80 and the integration of these local computations over space and time [21]. The homological scaffolds
81 summarises the role of network edges constituting the cycles during the filtration process; enabling to
82 identify edges belonging to multiple cycles and/or highly persistent cycles along the filtration. A hypothesis
83 tested in this study is that the edges supporting these mesoscopic network anti-structures will be well
84 positioned to bridge together segregated functional brain modules, rather than participate in densely
85 connected local networks.

86 The present study investigates the relationship between standard network metrics computed from dyadic
87 interactions in a functional brain network, and metric computed on the *persistence homological scaffold*
88 of the network. Toward this aim we generate a persistence scaffold from the whole-brain functional
89 connectivity data of healthy subjects recorded during resting-state fMRI. We then convert edge-persistence
90 scaffold values into a node-level measure termed *persistence scaffold strength (PSS)* which enables
91 comparisons between the persistence scaffold and local graph metrics computed on the original network.
92 We introduce this new measure because homological scaffold theory does not yet include node-level metrics
93 analogous to the topological centrality measures typically used in the analysis of functional brain networks.
94 We find that the unique mathematical attributes of the persistence homological scaffold may render it useful
95 for identifying key local nodes supporting the global integration of information processing directly from
96 functional neuroimaging data.

2 MATERIAL & METHODS

97 2.1 Data

98 2.1.1 Study Participants

99 Neuroimaging data were collected at CFIN, Aarhus University Hospital, Denmark, from 16 healthy right-
100 handed participants (11 men and 5 women, mean age: 24.7 ± 2.5). Participants with a history of psychiatric
101 or neurological disorders were excluded from participation in the study. The study was previously approved
102 by the Center of Functionally Integrative Neuroscience internal research board. The study was performed

103 in accordance with the Declaration of Helsinki ethical principles for medical research and ethics approval
104 was granted by the Research Ethics Committee of the Central Denmark Region (De Videnskabsetiske
105 Komiter for Region Midtjylland). Informed consent was obtained from all participants.

106 2.1.2 MRI data acquisition

107 MRI data were collected in one session on a 3T Siemens Skyra scanner. The parameters for the structural
108 MRI T1 scan were as follows: voxel size of 1 mm^3 ; reconstructed matrix size 256×256 ; echo time (TE) of
109 3.8 ms and repetition time (TR) of 2300 ms. The resting-state fMRI data were collected using whole-brain
110 echo planar images (EPI) with TR = 3030 ms, TE = 27 ms, flip angle = 90° , reconstructed matrix size =
111 96×96 , voxel size $2 \times 2 \text{ mm}$ with slice thickness of 2.6 mm and a bandwidth of 1795 Hz/Px. Seven minutes
112 of resting state fMRI data were acquired for each subject.

113 2.1.3 MRI data processing

114 We used the automated anatomical labeling (AAL) template [40] to parcellate the entire brain into
115 90 cortical and subcortical regions (45 for each hemisphere) which represented the nodes in functional
116 connectivity networks. The parcellation was conducted in the EPI native space. Linear registration was
117 performed using the FSL toolbox (www.fmrib.ox.ac.uk/fsl, FMRIB, Oxford) [37]. The EPI image was
118 co-registered to the T1-weighted structural image, and the T1-weighted image was coregistered to the T1
119 template of ICBM152 in MNI space. The resulting transformations were concatenated and inversed and
120 further applied to warp the AAL template from MNI space to the EPI native space, where interpolation
121 using nearest-neighbor method ensured that the discrete labelling values were preserved. Initial fMRI data
122 preprocessing was carried out using FEAT (FMRI Expert Analysis Tool) Version 6.00, part of FSL and
123 consisted of: motion correction using MCFLIRT; non-brain tissue removal using BET; spatial smoothing
124 using a Gaussian kernel of FWHM 5mm; grand-mean intensity normalisation of the entire 4D dataset by
125 a single multiplicative factor; high pass temporal filtering (Gaussian-weighted least-squares straight line
126 fitting, with $\sigma = 50.0\text{s}$).

127 2.1.4 Functional Connectivity Analysis

128 We used FSL to extract and average the time courses from all voxels within each AAL cluster. We then
129 used Matlab (The MathWorks Inc.) to compute the pairwise Pearson correlation between all 90 regions.
130 R -values were transformed to z -values via Fisher transformation, and the resulting z -values composed the
131 final 90×90 functional connectivity (FC) matrix. We averaged the FC matrices for all 16 participants to
132 obtain a group-averaged 90×90 FC matrix.

133 2.2 Persistent homology and scaffolds

134 The next two sections will introduce fundamental notions needed to understand persistent homology,
135 which is presented in the third section. Homological scaffolds are then defined and a toy example is
136 presented in the penultimate section. The last section exposes the open problem and implications of
137 the choice of a cycle's representative in the filtration. The workflow is illustrated in Fig. 2 and can be
138 summarised as follows: one starts from the data, that for the sake of generality we will assume to be a fully
139 connected, weighted and signed matrix. As the matrix is square and symmetrical, one can interpret it as an
140 undirected network adjacency matrix. The persistent homological features of the data are then computed
141 and finally summarised in the persistence and frequency scaffolds. These scaffolds can be seen as an edge
142 centrality measure, that emphasizes the role of an edge in the persistent homological characterisation of the
143 original data but they can also be considered as network in itself and analysed as such, as we define the

144 *PSS* in section 2.3.3. For a comprehensive introduction to persistent homology, the interested reader is
145 invited to consult [44, 10, 26].

146

147 2.2.1 Simplices, Simplicial Complex, and Holes

148 A *simplicial complex* can be seen as a generalisation of a graph, where interactions, instead of being
149 strictly between nodes, are between objects called *simplices* that generalise the notion of nodes. In the
150 present context, a node is a 0-dimensional simplex, an edge a 1-dimensional simplex, (representing a binary
151 interaction) a full triangle is a 2-dimensional simplex (representing ternary interactions), and so on for
152 higher dimensions. A *simplicial complex* is thus a type of topological space that is a collection of simplices
153 of any dimension (Fig.1).

154 There are many types of simplicial complexes. In this study, we focus on *clique complexes*, which can
155 be constructed from any network. In graph theory, a *clique* is a subset of vertices of a graph in which
156 every pair of vertices is adjacent. Thus a k -clique is a completely connected subgraph $K_k \subset G$, composed
157 by k nodes containing all the possible edges among its nodes. When representing a simplicial complex,
158 simplices are typically shaded, or filled in to identify them (Fig. 1). Importantly, upon identifying all the
159 simplices in a clique complex, structures called *holes* can remain, and these are the structures of interest
160 in this analysis (Fig.1). A hole of dimension k , or k -hole, is a hole bounded by simplices of dimension k .
161 In this paper, we focus on holes bounded by 1-dimensional boundaries, also called "cycles". In a clique
162 complex, a cycle is a minimal closed path of length greater than 3 (Fig. 1). This is due to the fact that each
163 clique corresponds to a full simplex so that a triangle is filled in. The set of k -holes defining a space is
164 described by the k -th homology group H_k . Each k -hole i is in turn represented by its generator $g_i^k \in H_k$.
165 Informally, generators are formed of elements of H_k that identify and can be used to construct the hole.

166

167 *Key concepts:* A clique complex is constructed from a network by identifying k cliques to $k - 1$
168 dimensional simplices. A clique complex can be described by its holes. A cycle is a hole of dimension 1
169 (Fig. 1).

170 2.2.2 Homology

171 One of the most studied problems in mathematics is that of defining a notion of similarity between
172 spaces. Intuitively, two spaces can be thought to be similar if we can transform one into the other via a
173 well-behaved transformation. In particular, if there exists a continuous bijective map, a homeomorphism,
174 that transforms one space into the other, then the two spaces are said to be homeomorphic. Such spaces are,
175 informally, topologically the same, and any of their properties that are conserved by homeomorphism are
176 are thus called *topological invariants*.

177

178 The homology group, or simply *homology*, is a property of a space which is based on the counting of
179 holes and their associated dimensions. As an analogy to homology, the reader can think of *The Hound of*
180 *the Baskervilles* by Sir Arthur Conan Doyle [17], where the non-manifestation of the hound one night was
181 as informative to Sherlock Holmes as its presence. Homology is a topological invariant which, as explained
182 above, means that it is a property of a space that is preserved by homeomorphisms and keeps the same
183 value whatever the representation of the system (i.e. the bijective map used to look at it). Thus, if two
184 spaces have the same homology, then they are topologically equivalent.

185

186 2.2.3 Persistent homology

187 The process of adding simplices to form a simplicial complex is called a filtration, and the filtration
 188 we use in this paper is the *weight clique rank filtration* [32]. It has been specifically designed to extract
 189 homological features from fully connected, weighted and signed networks. The filtration starts with a set
 190 of disconnected nodes. Then all the edges from the original network are sorted in descending order of
 191 magnitude and added one by one as 1-simplices to the complex. After each addition, the clique complex is
 192 constructed and its persistent homology computed. When a new cycle appears, it is tagged with a "birth
 193 time", β_i and when it disappears, it is tagged with a "death time", δ_i . The difference between the two time
 194 points defines its persistence π_i . It is important to note that when the starting network is fully connected, all
 195 the cycles eventually die along the filtration. While it is true that the order in which edges are introduced
 196 can depend on very small differences in the weights, the same small differences would alter the persistence
 197 or appearance of generators by a similarly small value hence ultimately producing small variations in the
 198 scaffold. This is a consequence of the robustness theorems for persistent homology, where one substitutes
 199 the usual metric with an extended semi-metric[3, 9, 10].

200

201 *Key concept:* The persistence of each cycle is measured using weight rank filtration.

202 2.2.4 Homological scaffolds

203 The homological scaffolds are secondary networks and were introduced in [31] as a mean to summarise
 204 part of the persistent homology of cycles information for the edges. As they localise the cycles on specific
 205 edges of the network, they can naturally be seen as edge centrality measures that characterise the importance
 206 of links in the original network through the filtration process, where the weights on the edges represent
 207 their centrality.

208

209 Two scaffolds are introduced to highlight different aspects of the importance of an edge in the network:
 210 the number of cycles an edge belongs to and the total persistence of the cycles it belongs to. The weights of
 211 the edges are defined as:

$$\omega_e^f = \sum_{g_j} \mathbf{1}_{e \in g_j} \quad (1)$$

212 for the frequency scaffold H_G^f , and

$$\omega_e^p = \sum_{g_j | e \in g_j} \pi_{g_j}, \quad (2)$$

213 for the persistence scaffold H_G^p .

214

215 The information given by the scaffolds has to be interpreted with care, see section 2.2.6 below
 216 for a full description of the limitations. The python library we developed for persistent homology
 217 analysis, that includes the weight rank clique filtration and the scaffolds generation is available at:
 218 <https://github.com/lordgrilo/Holes>.

219

220 *Key concept:* The homological scaffold measures the importance of edges relative to the number of cycles
221 they belong to and the persistence of these cycles. The present study focuses exclusively on the *persistence*
222 *scaffold*.

223 2.2.5 Example

224 Persistent homology and the computation of the scaffolds can be illustrated by a simple toy example,
225 which is described in the following lines and shown graphically in Fig. 3. For simplicity, some of the
226 edges have a weight of zero and are thus not represented. The first step is the filtration: edges are added
227 in decreasing order of magnitude. In the example, edges have five different weights. Accordingly, five
228 filtration steps are needed, and five associated clique complexes are formed. There are two cycles: one born
229 at step 2) and one born at step 3). By contrast, the edge added at step 4) does not define a new cycle. The
230 aforementioned cycles are both killed by the addition of the two edges at step 5). Their persistences are
231 summarized in the barcode below the filtration. The resulting scaffolds are on the right of the barcode: the
232 persistence scaffold (green) and frequency scaffold (blue). Inspecting the weights of both scaffolds, we
233 conclude that edge $\langle fc \rangle$ is the most important to support the homological structure of the network.

234 2.2.6 On the effect of the cycle representative

235 As illustrated by the present paper and [31], homological scaffolds can be quite informative, however
236 there is a caveat one has to be aware of when interpreting the results: the choice of a cycle's representative.
237 Persistent homology probes a dataset for its homological features that are persistent – more specifically
238 in the case treated in this paper, cycles. Cycles are topological objects and thus their "sizes" are not
239 uniquely defined, because the homology generators are defined as an equivalence class. Indeed, each cycle
240 corresponding to a certain homology generator can be stretched and deformed, while still remaining a valid
241 representative cycle. In practice, however, to identify homological properties of a topological space, one
242 has to recourse to a representation of the components of the simplices that bound it. In this setting, a hole
243 will be uniquely identified by the edges (or higher-dimensional simplices) forming its smallest boundary
244 at the time of its birth. During the filtration process, a cycle will potentially shrink due to the addition of
245 an edge. Although the shrinking has no topological meaning for the hole itself as it remains the same, its
246 representation changes, i.e. the specific edges forming its boundary change. The question "what is the best
247 representative of a cycle" is an open problem and the definition of *best* strongly depends on the problem at
248 hand.

249

250 In practice, however, this will have an impact. We used the software package javaplex [39] in our pipeline
251 for the implementation of persistent homology. It chooses a representative for a cycle and identifies it with
252 the entire lifetime of the cycle. This means that a unique set of edges will represent a cycle, regardless of
253 its possible contraction. This has a direct implication on the scaffolds, and means they are not well-defined.
254 This does not mean they are not informative, but rather that care has to be taken when interpreting the
255 meaning of the particular edges weight forming the scaffolds. The evolution of any cycle representative is a
256 combination of two possible situations:

- 257 1. A cycle shrinks by triadic closure,
- 258 2. a cycle is split into 2 smaller cycles.

259 These two possibilities are illustrated in Fig. 4, case i) on the top and case ii) on the bottom. Therefore,
260 one can monitor the original cycles' subgraphs evolutions as edges are added during the filtration to verify
261 how the cycles die and correctly interpret the homological scaffolds.

262 Practically, this means exploring the statistics of the holes and verify how they close. It is also important
 263 to note that the aforementioned phenomena are more likely to occur in cycles that are long lived.

264 2.3 Graph Theoretical Analysis

265 By construction, the graphs that we have considered for the standard graph analysis are unweighted,
 266 undirected, and do not contain self-loops. Their adjacency matrix A is therefore symmetric, and its elements
 267 are equal to 1 if nodes i and j are connected and zero otherwise.

268 2.3.1 Standard Graph Metrics in Binarized Graphs

269 We now briefly introduce the standard local centrality measures that were applied to the networks: degree
 270 centrality (DC), betweenness-centrality (BC), local efficiency (Eff) and participation coefficient (PC).
 271 Standard graph measures were calculated using the *Brain Connectivity Toolbox* in Matlab [34]. These
 272 metrics each capture different aspects of the contributions of a node to the network organization. To
 273 facilitate the interpretation of standard graph metrics, functional connectivity matrices were binarized at
 274 eleven statistical thresholds that give a network link density (D) in the range $[0.10, 0.60]$ in increments of
 275 0.05, eliminating the weakest links in the network. This thresholding approach was performed using the
 276 *threshold_proportional* function of the *Brain Connectivity Toolbox*.

277

278 The degree centrality is a measure of the total number of connections that a node has. It therefore depends
 279 on the direct neighborhood of the node. For a node j within a binarized network comprising N nodes,
 280 degree centrality is defined as:

$$DC(j) = \sum_{i=1}^N A_{i,j} \quad (3)$$

281 The betweenness-centrality of a node measures how many of the shortest paths between all other node
 282 pairs pass through it and is a measure of its importance when routing information in the network. By
 283 contrast to the degree, BC is dependent of the overall topology of the rest of the network beyond the direct
 284 neighborhood of a node. For a node k it is defined as:

$$BC(k) = \sum_{i \neq j \neq k, i, j=1}^N \frac{\hat{\sigma}_{i,j}(k)}{\hat{\sigma}_{i,j}} \quad (4)$$

285 where $\hat{\sigma}_{i,j}(k)$ is the number of shortest paths going from node i to node j through node k , and $\hat{\sigma}_{i,j}$ is the
 286 total number of shortest paths going from node i to node j .

287 The local efficiency of a node k computes how well the neighbors of a node are connected together. That
 288 is, the inverse of the average shortest path length connecting the neighbors of that vertex:

$$Eff(k) = \frac{2}{Nn(n-1)} \sum_{i \in G}^n \sum_{i < j \in G}^n \frac{1}{d_{i,j}} \quad (5)$$

289 where n is the number of neighbors of a node k .

290

291 In addition, a community detection algorithm based on modularity (*Louvain method with finetuning*[4])
 292 was applied to the adjacency matrix with $D = 0.40$, and identified six communities for the partition

293 optimising the modularity function. The participation coefficient was then calculated for each node in
 294 this network. The participation coefficient compares the degree of a given node to nodes in all other
 295 communities with the number of links it has within its own cluster. Nodes with a high participation
 296 coefficient are therefore expected to play an important role in binding different communities together and
 297 hence contribute to global integration. This measure therefore provides additional information about a
 298 node's role in the network topology which cannot be inferred from measures of topological centrality alone.
 299 It is defined as:

$$PC_i = 1 - \sum_{c=1}^{N_C} \left(\frac{k_{C_i}}{k_i} \right)^2, \quad (6)$$

300 where k_i is the degree of node i and k_{C_i} its degree limited to cluster C .

301 2.3.2 Weighted Network Analysis

302 As a follow-up analysis, we explored the relationship between the *PSS* and the weighted counterparts
 303 of the same three graph metrics employed in the original graph analysis described in section 2.3.1: the
 304 nodal *strength* (weighted counterpart of degree), the weighted betweenness centrality (*wt - BC*) and
 305 the weighted local efficiency (*wt - Eff*). By definition, the computation of these measures on a fully
 306 connected weighted graph does not rely on the *ad hoc* thresholding of the FC matrix. The mathematical
 307 formulation of the weighted version of the metrics are the same as in the unweighted case. For the nodal
 308 strength, one sums up the weights of the links connected to a node:

$$SC(j) = \sum_{i=1}^N W_{i,j}. \quad (7)$$

309 For the weighted versions of betweenness centrality and efficiency, the difference resides in the definition
 310 of the shortest path. In the BCT implementation, the shortest path is computed via a breadth-first search
 311 algorithm that follows the links with the smallest weight [5].

312 2.3.3 Definition of PSS

313 Lastly, we define a new centrality measure for the homological scaffolds, the nodal *persistence scaffold*
 314 *strength (PSS)*. It is essentially the strength of a node, i.e. the sum of the weights of its links, in the
 315 persistence scaffold H_G^p . We gave it a different name to clearly differentiate its meaning as a measure
 316 obtained from the persistent homology procedure instead of pairwise interactions between edges and
 317 vertices. It is defined as:

$$PSS(j) = \sum_{i=1}^N H_{G,i,j}^p \quad (8)$$

318 The *PSS* thus compresses into a scalar information about the persistence of cycles passing through a given
 319 node. The *PSS* may thereby effectively capture the combination of a nodes central position in the network
 320 and the relative lack of connectivity amongst its local neighbourhood. Moreover, as outlined above, the
 321 *PSS* does not rely on *ad hoc* thresholding of the functional connectivity matrix and therefore includes
 322 information from all the edges in the network. This is an important distinction between the *PSS* and the
 323 topological centrality metrics traditionally measures applied to functional neuroimaging data.

324 2.3.4 Definition of Functional Hubs

325 Node-level values were calculated for the *PSS* measure as well as standard graph centrality measures.
326 As indicated above, the *PSS* does not require *a priori* thresholding of the functional connectivity matrix.
327 However, for the computation of local graph measures (*DC*, *Eff* and *BC*), we calculated the node-level
328 metric values at each of eleven different thresholds over the $D = [0.10, 0.60]$ range. This curve was then
329 integrated to yield a single nodal metric value that is independent of the threshold. The highest-ranking
330 nodes (termed "hubs" for concision) were then identified for each of measure under study. They were
331 defined as those nodes with a metric value larger than 1 standard deviation from the mean of their respective
332 distribution.
333

3 RESULTS

334 3.1 Relationship between nodal *PSS* and standard graph metrics

335 3.1.1 Topological centrality in binary networks

336 The main objective of this analysis was to examine the relationship between standard topological centrality
337 measures described above; *DC*, *BC*, *Eff* and the nodal *PSS*. This was done by computing bivariate
338 correlations between the standard graph metric values and nodal *PSS* across the threshold range applied to
339 the functional connectivity matrix. The *R*-values and *p*-values for each analysis are listed in supplementary
340 figures S1a and S1b. It is important to note that while different FC network thresholds were used for
341 the standard graph analysis, the input FC matrix for the persistent homology analysis did not require *a*
342 *priori* thresholding, which is a potential strength of this methodology. In order to verify that the reported
343 associations between nodal *PSS* and standard metric values at a given threshold were not simply driven by
344 the direct connectivity of network nodes, we also examined the correlations *DC* vs *BC*, *DC* vs *Eff* and
345 *BC* vs *Eff* as control conditions (Fig. 5).

346 *PSS* vs *DC*: The positive correlation between *PSS* and *DC* was significant at all thresholds under
347 study, although it was consistently weaker than the correlation of *PSS* vs *BC*.

348 *PSS* vs *BC*: The *PSS* showed strong and also statistically significant positive correlations with the *BC*
349 metric at all thresholds under study. This indicates that *PSS* is associated with a node's tendency to be
350 part of shortest paths between node pairs in the network.

351 *PSS* vs *Eff*: Conversely, a strong and significant *negative* correlation was observed between the *PSS*
352 and *Eff* metrics at all but one threshold, showing that high *PSS* nodes generally avoid densely connected
353 neighborhood clusters. These results are illustrated in the top panel of Figure 5.

354 *DC* vs *BC*: By contrast to *PSS* vs *BC*, the *DC* vs *BC* correlation failed to reach statistical significance
355 at 5 of the 11 thresholds under study. When the relationship did reach statistical significance at some of the
356 higher network densities, the *DC* vs *BC* correlations remained on average weaker than *PSS* vs *BC* over
357 the same threshold range.

358 *DC* vs *Eff*: The *DC* vs *Eff* correlation also showed a threshold-dependent profile. Significant positive
359 correlations were observed at some of the lower densities in the $D = [0.1, 0.2]$ range which contrasted with
360 the *negative* correlations between *PSS* vs *Eff* observed at these same thresholds. *DC* vs *Eff* did not
361 reach statistical significance at any of the thresholds exceeding $D > 0.35$.

362 *BC vs Eff*: Finally, the negative correlation between the *BC* and *Eff* metrics was qualitatively similar
363 to the *BC vs PSS* correlation over the threshold range. However, *BC vs Eff* did not reach statistical
364 significance at the lowest network density of $D = 0.1$ and the negative correlation strengths at higher
365 densities were overall stronger (and less stable) for *BC vs Eff* than *PSS vs BC*. These results are
366 graphically represented in the bottom panel of Figure 5.

367 3.1.2 Topological centrality in weighted networks

368 As a follow-up analysis, the relationships between the *PSS* and the weighted counterparts of the
369 metrics used in the original analysis were also studied. These included the nodal *strength*, weighted
370 betweenness-centrality (*wt - BC*) and weighted efficiency (*wt - Eff*).

371 *strength vs PSS*: There was a borderline significant positive correlation between the nodal strength in
372 the weighted network and the *PSS*: $R = 0.21$, $n = 90$, $p = 0.046$.

373 *wt - BC vs PSS*: The positive correlation between *wt - BC vs PSS* was stronger than *strength vs*
374 *PSS* and highly significant: $R = 0.39$, $n = 90$, $p < 0.01$; consistent with the results of the binary graph
375 analysis.

376 *wt - Eff vs PSS*: There was a significant *positive* correlation between *PSS vs wt - Eff*: $R = 0.23$,
377 $n = 90$, $p = 0.03$. This relationship was opposite to that observed in the binary network analysis where
378 *PSS vs Eff* instead showed a strong *negative* association at all thresholds under study.

379 3.1.3 Participation Coefficient

380 For the network with an intermediate density of $D = 0.40$, a community detection algorithm was applied
381 to the data and the participation coefficient (*PC*) was computed for each node in the network. A significant
382 positive correlation was revealed between *PC* and *PSS*, $R = 0.32$, $n = 90$, $p < 0.01$. This indicated that
383 the *PSS* measure also reflects the tendency of a node to act as a bridge across communities in distributed
384 brain networks.

385 3.2 Identification of functional hubs using the *PSS* and standard graph measures

386 We now explain the results shown in Fig. 6 and Fig. 7. Functional hubs were identified on each of the
387 *PSS*, *DC*, *Eff* and *BC* measures using the procedure outlined in section 2.3.4. Fourteen AAL regions
388 (out of 90) were identified as hubs on the *PSS* measure. The most important overlap was observed between
389 the *PSS*-hubs and the *DC*-hubs (5/14) and the second-most important overlap was between the *PSS*-hubs
390 and *BC*-hubs (4/14). We note that this was the case despite the presence of a stronger positive correlation
391 between *PSS vs BC* than *PSS vs DC* at all the thresholds under consideration. As expected, *Eff*-hubs
392 showed the least amount of overlap with the *PSS*-hubs, consistent with the strong negative correlation
393 between these two measures.

4 DISCUSSION

394 Persistent homology provides a window into the global organization of the edges' weights fabric of a
395 graph. The present results indicate that persistence homological scaffolds may be useful objects to consider
396 in functional neuroimaging research. The persistence scaffold notably circumvents the need for *ad hoc*
397 thresholding of the functional connectivity matrix and is constructed using the data of all the edges present
398 in the original network. Moreover, the concept of *simplicial complexes* upon which the persistence scaffold
399 is built allows one to describe relations between distributed sub-populations of network elements consistent

400 with the brain's encoding of information in distributed networks, and is not restricted to dyadic associations
401 between region pairs.

402

403 In order to study the relationship between standard network metrics and on the persistence homological
404 scaffold, we calculated the strength of each node in the persistence scaffold and termed this novel measure
405 the persistence scaffold strength (*PSS*). The *PSS* measure hence differs in important ways from the
406 standard graph metrics used in neuroimaging studies as it includes information from seemingly unimportant
407 edges with weak weights in the network, and considers the contributions of mesoscopic structures ("cycles")
408 to the network organization, rather than edge-vertex interactions. We then examined how *PSS* relates to
409 some of the local binarized and weighted graph theoretical metrics typically employed in neuroimaging
410 studies.

411

412 Of the binary graph metrics under study, *PSS* showed the strongest positive correlation with the
413 betweenness-centrality metric (*BC*) across the entire threshold range. Even when controlling for the node
414 degree by means of a partial correlation analysis, the positive association between *PSS* and *BC* remained
415 highly significant. This suggested that high *PSS* nodes are likely to contribute to the binding of information
416 across different sources in the brain by creating shortest paths between node pairs. Conversely, a strong
417 negative correlation was observed between *PSS* and local efficiency (*Eff*), and indicates that nodes
418 with a high *PSS* are unlikely to participate in strongly integrated local networks. To further explore the
419 association between the *PSS* measure and functional integration, we conducted a modularity analysis and
420 computed the participation coefficient (*PC*) of network nodes. A strong positive correlation between *PC*
421 and *PSS* was found in the network under study. Nodes with a high participation coefficient preferentially
422 make connections to network communities other than their own, consistent with network roles in global
423 integration.

424 Taken together, these observations lead to an understanding of the meaning of this new centrality measure
425 and on the interpretation of persistent homological scaffold. The tendency of high *PSS* nodes to bind
426 topologically remote modules in the brain whilst simultaneously avoiding clustered neighbourhood reflects
427 the significance of persistent homology in resting-state fMRI data. *PSS* therefore captures different aspects
428 of global network organisation in a natural index that does not rely on any weighted average of classic
429 graph metrics, and that extracts this information directly from the data. We also note that although for
430 interpretational purposes we limited ourselves to the study of the first homology group, the *persistence*
431 *scaffold strength* can easily be generalised to higher dimensions, where it would capture aspects of the
432 network organisation that are not reflected at all by traditional network metrics.

433 When bypassing the thresholding step and instead comparing the *PSS* to the *weighted* counterparts
434 of the standard graph measures computed on the fully connected network, the results for *strength* and
435 *wt - BC* were broadly consistent with those of the binarized networks. As in the binary network analysis,
436 the *strength vs PSS* correlation was positive and significant, but weaker than the *wt - BC vs PSS*
437 correlation. However a significant *positive* correlation was observed for the *PSS vs wt - Eff* correlation
438 in the weighted network, which was inconsistent with the results of the thresholded network analysis where
439 the binarized version of the two metrics were actually *negatively* correlated at every threshold under study.
440 This exemplifies that the generalisation of a binary graph metric to a fully connected weighted network
441 does not imply its specialization.

442 Finally, we note that the nodal *PSS* does not merely recapitulate the betweenness-centrality metric.
443 Although the correlation between *PSS* and *BC* measures was significant at all thresholds under study in
444 the binary networks analyses, only 4 of the 14 highest ranking *PSS* nodes overlap with the hubs identified
445 on the *BC* metric (Fig. 6). This may be explained by the fact that some nodes ranking highly on the
446 betweenness-centrality metric concurrently participate in strongly connected neighborhood clusters; their
447 respective edges would thus form clique complexes at an early stage in the filtration, leading to low *PSS*
448 value. Moreover, the value of the correlation between *PSS* and *BC* was around $R = 0.4$ in both the
449 binarized and weighted network analyses, which further suggests that the *PSS* and *BC* do not reflect
450 identical network attributes.

451 The highest-ranking regions on the *PSS* measure (Figs 6-7) were distributed across the brain, consistent
452 with potential roles in the global integration of local networks. There was nevertheless a tendency for the
453 *PSS* hubs to belong to frontal cortical areas (middle & superior frontal gyri, precentral gyrus, rolandic
454 operculum, cingulate), and subcortical structures (amygdala, globus pallidum, caudate nucleus). In the
455 posterior brain, *PSS*-hubs within the parietal lobe included the inferior and superior divisions of the
456 parietal gyrus but did not include midline parietal structures. In the occipital lobe, a visual association area
457 located in the superior occipital cortex ranked highly as a *PSS* hub, as did the calcarine fissure which
458 includes part of the primary visual cortex (V1). We note that V1, which also ranked highly on the *DC*
459 metric in this study, has previously been shown to engage in distributed networks thought to support mental
460 imagery during the resting-state [43]. Interestingly, no subdivision of the temporal cortices were included
461 amongst *PSS*-hubs, despite several of these regions ranking highly on the *DC* measure.

462

463 We also paid attention to the special case of high-ranking *PSS* nodes which did **not** qualify as "hubs"
464 on any of the three standard topological centrality measures (*DC*, *Eff*, *BC*). This subset of nodes was
465 anatomically restricted to the lateral frontal and parietal cortices. They included the middle and superior
466 frontal gyri, as well as inferior and superior sections of parietal gyri. These findings would suggest that,
467 relative to standard topological centrality metrics, the *PSS* may be particularly sensitive to the network
468 activity of frontal and parietal association areas located on the lateral surface of the brain. This would be
469 consistent with the established role of these regions towards supporting high-level cognitive and behavioral
470 functions requiring the large-scale coordination of network elements. The relative importance of *PSS*-hubs
471 towards the information processing capacities of the brain should notably be assessed in future studies by
472 means of virtual lesions in whole-brain computational models [13, 14, 42].

473

474 It has now become well recognized that the brain performs local computations in segregated modules
475 that become seamlessly integrated over space and time to support high-level functions necessary for
476 survival. Some brain regions are likely to play a more critical role than others towards enabling the global
477 integration of information. The exact identities of these regions and the optimal experimental approaches
478 for identifying them remain unclear. However recent evidence would suggest that integrative nodes, such
479 as those potentially identified via the persistence homological scaffold, require metastability for maximal
480 exploration of the full dynamic repertoire of the brain [22]. Previous research has employed diffusion tensor
481 imaging (DTI) and graph theoretical analysis to identify a subset of hubs which forms a central core or
482 "rich-club" that has been suggested to be important for global brain integration by linking together spatially
483 remote network communities [41]. Yet, the mapping of a structural network architecture that can plausibly
484 support segregation and integration does not describe the causal mechanisms and/or activity dynamics that
485 actually underlie functional segregation and integration of information [14]. The identification of integrator

486 hubs directly from *functional* neuroimaging data using the homological scaffold may be particularly
487 valuable in this regard.

488

489 The application of computational topology analysis to functional neuroimaging data is a novel avenue of
490 research, and the physiological significance of homological scaffolds and related measures remains unclear.
491 Given that high *PSS* nodes participate in a large proportion of cycles along the filtration, such nodes
492 may be well positioned to contribute to a specific type of integration where, for example, a given neural
493 pathway diverges than re-converges. Examples of such pathways include the dorsal/ventral visual streams
494 and the well-defined cortico-basal loops between the basal ganglia and motor cortex. Further studies will
495 be needed to test these hypotheses with specificity, but we nevertheless point out that the identification of
496 both visual areas as well as basal ganglia and cortical motor areas amongst the *PSS*-hubs in the present
497 analysis supports this idea.

498

499 Whilst the present results suggest that high-ranking *PSS* nodes could be well positioned to support the
500 integration of information across segregated brain modules, further studies will be needed to confirm this
501 observation. One potential approach would be to apply recently developed measures of perturbational
502 integration and segregation in a whole-brain computational model. Previous work has shown that, by
503 perturbing *in silico* neural dynamics by a random set of Gaussian inputs, one can estimate and the amount
504 of integration in the system calculated after each perturbation. In this context, perturbational integration
505 is defined by considering the length of the largest connected component of the functional network as an
506 estimate of the amount of integration in the system after each perturbation, as described in detail in [14].
507 One would therefore expect virtual lesions to high-*PSS* nodes to have a particularly profound impact on the
508 system's integration capabilities, relative to randomly selected network nodes. Another possibility would
509 be to investigate changes in *PSS* hubs assignment and distributions in clinical syndromes characterized by
510 disordered functional integration at the whole-brain scale, such as schizophrenia[25, 1]. Both approaches
511 could help determine to what extent *PSS*-hubs support the integration of network elements, and potentially
512 provide useful insights into the neurobiological attributes of topologically central brain regions in the
513 homological scaffold.

514

515 Another limitation of this study, as mentioned in section 2.2.6, is the choice of the representative cycles
516 for homology classes, which could result in selecting edges that do not belong to the shortest cycle around
517 a certain hole. A possible way around this limitation would be to perform an *a posteriori* analysis of
518 the cycles, in which one controls for the evolution of the subgraph's transitivity (as done in [31]). One
519 could also consider employing computationally cumbersome techniques to track the shortest path across
520 the filtration and then update the scaffold accordingly [16, 15]. Further work is needed to establish which
521 protocol would be most suited to the specific case of fMRI networks. Our results on network communities
522 nevertheless suggest that the cycle choice issues might not be so critical in our study and potentially lead to
523 a stronger *PSS* interpretation. Indeed network communities, being densely connected internally and strong
524 information integrators, likely constitute the network regions where connected triangle components reside
525 and thus the regions where different representative cycle choices are possible. Moreover, scaffold hubs
526 already tend to have large participation coefficients suggesting that they behave as information brokers
527 between these communities and are therefore, although imperfectly, capturing the large-scale homological
528 structure.

529 In summary, the present study has explored the relationship between standard network metrics in
530 functional brain network and the persistence homological scaffold derived from the same fMRI dataset.
531 The computation of a local graph measure on the persistence homological scaffolds (*PSS*) differs from
532 standard applications of graph theory to functional neuroimaging data as the scaffolds are not derived
533 from typical dyadic interactions between network elements, and consider information from all edges in
534 the network. The results suggest that topologically central nodes in the persistence scaffold may play
535 important roles towards supporting the functional integration of information across brain modules. Future
536 work should investigate the sensitivity of the homological scaffolds and derived measures to disease-related
537 changes in brain function as well as the specific type of integration performed by the strongest edges and
538 nodes in the scaffolds.

DISCLOSURE/CONFLICT-OF-INTEREST STATEMENT

539 The authors declare that the research was conducted in the absence of any commercial or financial
540 relationships that could be construed as a potential conflict of interest.

AUTHOR CONTRIBUTIONS

541 L-D.L., P.E., M.L.K., F.E.T. designed the study. T.V.H., H.M.F., M.L.K. collected and processed the
542 fMRI data. P.E., G.P., F.V. developed and implemented the persistence homological scaffolds methodology
543 essential to this study. L-D.L., H.M.F. performed the graph theoretical analysis of the data. P.E., L-D.L.,
544 T.V.H. made the figures. P.E., G.P., F.V. and L-D.L. wrote the methods section. L-D.L. wrote the results
545 section. L-D.L. and P.E. wrote the introduction and discussion sections, with editorial guidance from
546 M.L.K., F.E.T. and G.D.

ACKNOWLEDGMENTS

547 L-D.L. is supported by the Canadian Institutes of Health Research (CIHR), the Canadian Centennial
548 Scholarship Fund, and a scholarship award from Hertford College (University of Oxford). M.L.K. is
549 supported by European Research Council (ERC) Consolidator Grant: CAREGIVING (615539). F.E.T. and
550 P.E. are supported by a PET Methodology Programme grant from the Medical Research Council UK (ref no.
551 G1100809/1). G.D. is supported by ERC Advanced Grant: DYSTRUCTURE (295129) and by the Spanish
552 Research Project PSI2013-42091-P. G.P. and F.V. are supported by the TOPDRIM project supported by the
553 Future and Emerging Technologies programme of the European Commission under Contract IST-318121.

REFERENCES

- 554 [1] Alexander-Bloch, A. F., Gogtay, N., Meunier, D., Birn, R., Clasen, L., Lalonde, F., et al.
555 (2010). Disrupted modularity and local connectivity of brain functional networks in childhood-onset
556 schizophrenia. *Frontiers in systems neuroscience* 4, 147
- 557 [2] Bassett, D. S., Nelson, B. G., Mueller, B. A., Camchong, J., and Lim, K. O. (2012). Altered resting
558 state complexity in schizophrenia. *Neuroimage* 59, 2196–2207
- 559 [3] Bauer, U. and Lesnick, M. (2014). Induced matchings of barcodes and the algebraic stability of
560 persistence. In *Proceedings of the Thirtieth Annual Symposium on Computational Geometry* (New
561 York, NY, USA: ACM), SOCG'14, 355:355–355:364. doi:10.1145/2582112.2582168

- 562 [4] Blondel, V. D., Guillaume, J.-L., Lambiotte, R., and Lefebvre, E. (2008). Fast unfolding of
563 communities in large networks. *Journal of Statistical Mechanics: Theory and Experiment* 2008,
564 P10008–13
- 565 [5] Brandes, U. (2001). A faster algorithm for betweenness centrality*. *The Journal of Mathematical*
566 *Sociology* 25, 163–177
- 567 [6] Bullmore, E. and Sporns, O. (2009). Complex brain networks: graph theoretical analysis of structural
568 and functional systems. *Nature Reviews Neuroscience* 10, 186–198
- 569 [7] Bullmore, E. and Sporns, O. (2012). The economy of brain network organization. *Nature Reviews*
570 *Neuroscience* 13, 336–349
- 571 [8] Buzsáki, G. and Draguhn, A. (2004). Neuronal oscillations in cortical networks. *science* 304,
572 1926–1929
- 573 [9] Chazal, F., de Silva, V., Glisse, M., and Oudot, S. (2012). The structure and stability of persistence
574 modules. *ArXiv e-prints*
- 575 [10] Cohen-Steiner, D., Edelsbrunner, H., and Harer, J. (2007). Stability of persistence diagrams. *Discrete*
576 *& Computational Geometry* 37, 103–120
- 577 [11] Cole, M. W., Yarkoni, T., Repovš, G., Anticevic, A., and Braver, T. S. (2012). Global connectivity
578 of prefrontal cortex predicts cognitive control and intelligence. *The Journal of Neuroscience* 32,
579 8988–8999
- 580 [12] Csermely, P. (2004). Strong links are important, but weak links stabilize them. *Trends in biochemical*
581 *sciences* 29, 331–334
- 582 [13] Deco, G. and Kringelbach, M. L. (2014). Great expectations: using whole-brain computational
583 connectomics for understanding neuropsychiatric disorders. *Neuron* 84, 892–905
- 584 [14] Deco, G., Tononi, G., Boly, M., and Kringelbach, M. L. (2015). Rethinking segregation and integration:
585 contributions of whole-brain modelling. *Nature Reviews Neuroscience*
- 586 [15] Dey, T. K., Hirani, A. N., and Krishnamoorthy, B. (2011). Optimal homologous cycles, total
587 unimodularity, and linear programming. *SIAM Journal on Computing* 40, 1026–1044. doi:10.1137/
588 100800245
- 589 [16] Dey, T. K., Sun, J., and Wang, Y. (2011). Approximating cycles in a shortest basis of the first homology
590 group from point data. *Inverse Problems* 27, 124004
- 591 [17] Doyle, A. C. (1998). *The hound of the Baskervilles* (Oxford University Press)
- 592 [18] Garrison, K. A., Scheinost, D., Finn, E. S., Shen, X., and Constable, R. T. (2015). The (in) stability of
593 functional brain network measures across thresholds. *NeuroImage*
- 594 [19] Giusti, C., Ghrist, R., and Bassett, D. S. (2016). Two’s company, three (or more) is a simplex:
595 Algebraic-topological tools for understanding higher-order structure in neural data. *arXiv preprint*
596 *arXiv:1601.01704*
- 597 [20] Granovetter, M. S. (1973). The strength of weak ties. *American journal of sociology* , 1360–1380
- 598 [21] Hansen, E. C., Battaglia, D., Spiegler, A., Deco, G., and Jirsa, V. K. (2015). Functional connectivity
599 dynamics: Modeling the switching behavior of the resting state. *NeuroImage* 105, 525–535
- 600 [22] Kringelbach, M. L., McIntosh, A. R., Ritter, P., Jirsa, V. K., and Deco, G. (2015). The rediscovery of
601 slowness: Exploring the timing of cognition. *Trends in Cognitive Sciences* 19, 616–628
- 602 [23] Lord, L.-D., Allen, P., Expert, P., Howes, O., Broome, M., Lambiotte, R., et al. (2012). Functional
603 brain networks before the onset of psychosis: a prospective fmri study with graph theoretical analysis.
604 *NeuroImage: Clinical* 1, 91–98

- 605 [24] Lord, L.-D., Allen, P., Expert, P., Howes, O., Lambiotte, R., McGuire, P., et al. (2011). Characterization
606 of the anterior cingulate's role in the at-risk mental state using graph theory. *Neuroimage* 56,
607 1531–1539
- 608 [25] Lynall, M.-E., Bassett, D. S., Kerwin, R., McKenna, P. J., Kitzbichler, M., Muller, U., et al. (2010).
609 Functional connectivity and brain networks in schizophrenia. *The Journal of Neuroscience* 30,
610 9477–9487
- 611 [26] Munkres, J. R. (1984). *Elements of algebraic topology*, vol. 2 (Addison-Wesley Reading)
- 612 [27] Onnela, J.-P., Saramäki, J., Hyvönen, J., Szabo, G., Kaski, K., Kertész, J., et al. (2007). Structure and
613 tie strengths in mobile communication networks. *Proceedings of the National Academy of Sciences* ,
614 1–5
- 615 [28] Onnela, J.-P., Saramäki, J., Hyvönen, J., Szabó, G., Lazer, D., Kaski, K., et al. (2007). Structure and
616 tie strengths in mobile communication networks. *Proceedings of the National Academy of Sciences*
617 104, 7332–7336
- 618 [29] Pajevic, S. and Plenz, D. (2012). The organization of strong links in complex networks. *Nature*
619 *Physics* 8, 429–436
- 620 [30] Pandit, A. S., Expert, P., Lambiotte, R., Bonnelle, V., Leech, R., Turkheimer, F. E., et al. (2013).
621 Traumatic brain injury impairs small-world topology. *Neurology* 80, 1826–1833
- 622 [31] Petri, G., Expert, P., Turkheimer, F., Carhart-Harris, R., Nutt, D., Hellyer, P., et al. (2014). Homological
623 scaffolds of brain functional networks. *Journal of The Royal Society Interface* 11, 20140873
- 624 [32] Petri, G., Scolamiero, M., Donato, I., and Vaccarino, F. (2013). Topological Strata of Weighted
625 Complex Networks. *PLoS ONE* , 1–8
- 626 [33] Power, J. D., Cohen, A. L., Nelson, S. M., Wig, G. S., Barnes, K. A., Church, J. A., et al. (2011).
627 Functional network organization of the human brain. *Neuron* 72, 665–678
- 628 [34] Rubinov, M. and Sporns, O. (2010). Complex network measures of brain connectivity: uses and
629 interpretations. *Neuroimage* 52, 1059–1069
- 630 [35] Schneidman, E., Berry, M. J., Segev, R., and Bialek, W. (2006). Weak pairwise correlations imply
631 strongly correlated network states in a neural population. *Nature* 440, 1007–1012
- 632 [36] Schwarz, A. J. and McGonigle, J. (2011). Negative edges and soft thresholding in complex network
633 analysis of resting state functional connectivity data. *Neuroimage* 55, 1132–1146
- 634 [37] Smith, S. M., Jenkinson, M., Woolrich, M. W., Beckmann, C. F., Behrens, T. E., Johansen-Berg, H.,
635 et al. (2004). Advances in functional and structural mr image analysis and implementation as fsl.
636 *Neuroimage* 23, S208–S219
- 637 [38] Sporns, O. (2013). Network attributes for segregation and integration in the human brain. *Current*
638 *opinion in neurobiology* 23, 162–171
- 639 [39] Tausz, A., Vejdemo-Johansson, M., and Adams, H. (2011). Javaplex: A research software package for
640 persistent (co) homology. *Software available at <http://code.google.com/javaplex>*
- 641 [40] Tzourio-Mazoyer, N., Landeau, B., Papathanassiou, D., Crivello, F., Etard, O., Delcroix, N., et al.
642 (2002). Automated anatomical labeling of activations in spm using a macroscopic anatomical
643 parcellation of the mni mri single-subject brain. *Neuroimage* 15, 273–289
- 644 [41] van den Heuvel, M. P. and Sporns, O. (2011). Rich-club organization of the human connectome. *The*
645 *Journal of neuroscience* 31, 15775–15786
- 646 [42] Váša, F., Shanahan, M., Hellyer, P. J., Scott, G., Cabral, J., and Leech, R. (2015). Effects of lesions on
647 synchrony and metastability in cortical networks. *NeuroImage* 118, 456–467
- 648 [43] Wang, K., Jiang, T., Yu, C., Tian, L., Li, J., Liu, Y., et al. (2008). Spontaneous activity associated with
649 primary visual cortex: a resting-state fmri study. *Cerebral cortex* 18, 697–704

- 650 [44] Zomorodian, A. and Carlsson, G. (2005). Computing persistent homology. *Discrete & Computational*
651 *Geometry* 33, 249–274

Provisional

FIGURES

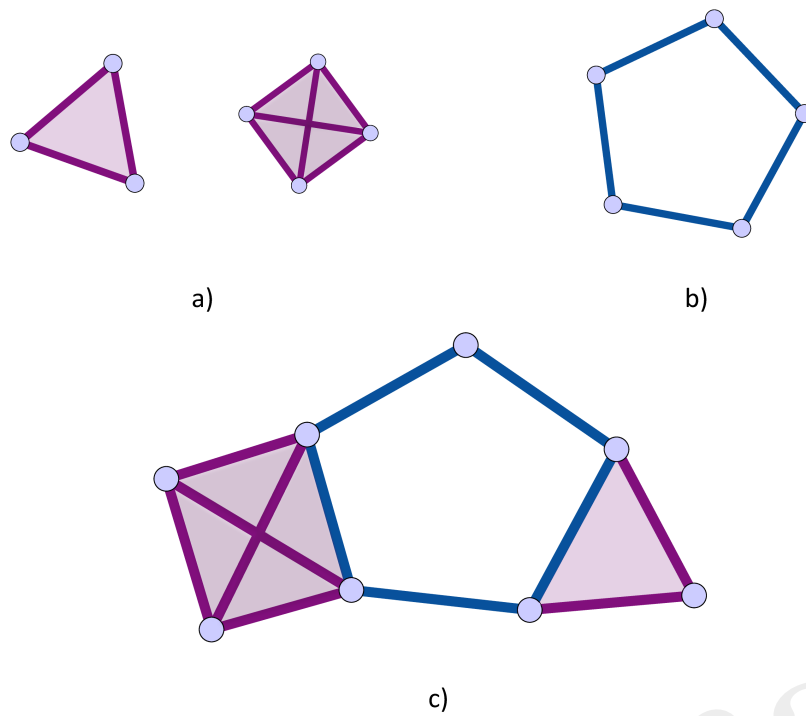


Figure 1. Illustrations of cliques, simplices, holes and clique complex. The simplices are shaded for identification. **a)** 3 and 4-cliques, which are associated to 2 and 3-dimensional simplices. **b)** a 1-dimensional hole, or cycle, is a closed path of edges of length greater than 3. **c)** Combining the elements of a) and b) following the rules in 2.2.1, one can produce a clique complex with one 1-dimensional hole. All simplices in this figure are shaded as is customary.

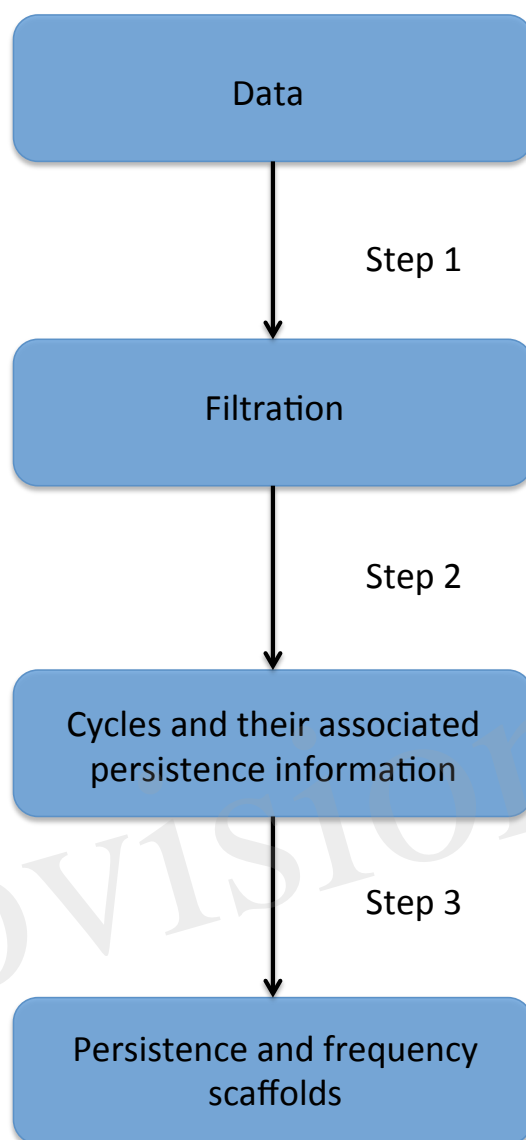


Figure 2. Description of the four stages of the persistent homology and homological scaffolds analysis workflow. **The data** consist of a fully connected weighted network. **The filtration** is produced using the weight clique rank filtration. **The persistent homology** of the filtration is computed, and each cycle (or 'hole') is endowed with a birth and death time. **The homological scaffolds** are generated using the information from persistent homology

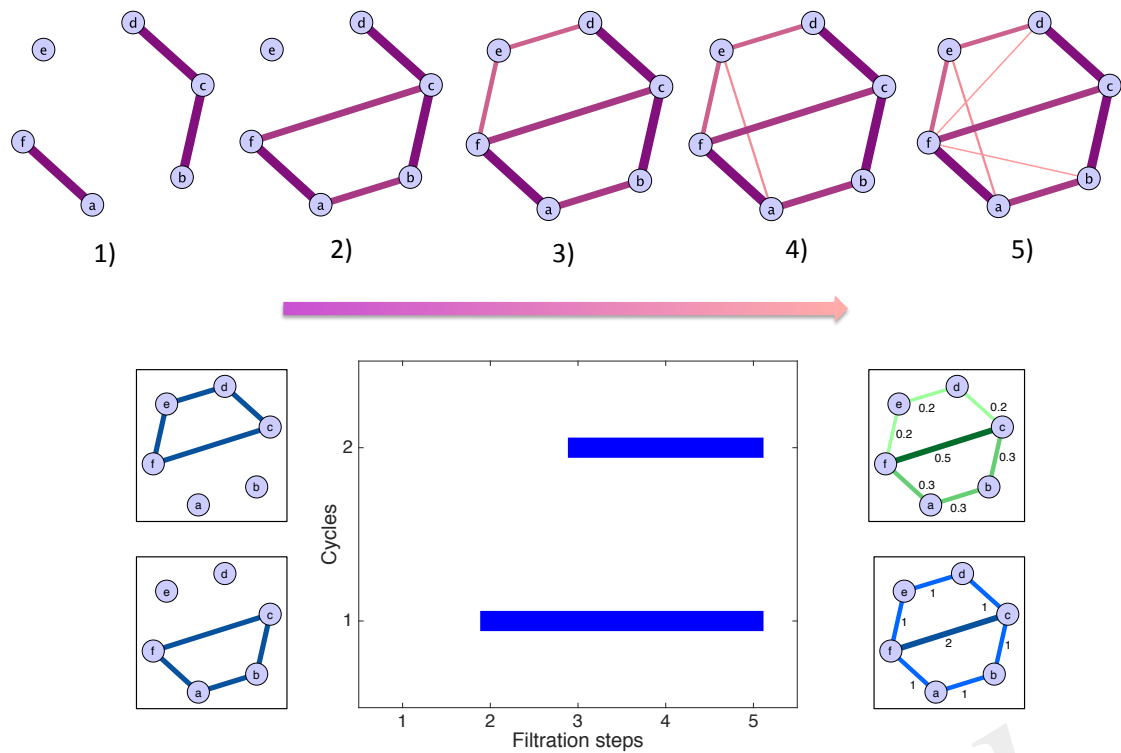


Figure 3. Toy example illustrating the generation of the homological scaffolds. **On top** The filtration: edges are added in decreasing order of weight (thickness and colour represent the weights) to arrive at the original network at step 5). **Bottom middle** The barcode encoding the persistence of the two cycles $\langle abc f \rangle$ and $\langle c d e f \rangle$. **Bottom right** The persistence (green) and frequency (blue) scaffolds, summarising the role of the edges in the cycles present during the filtration.

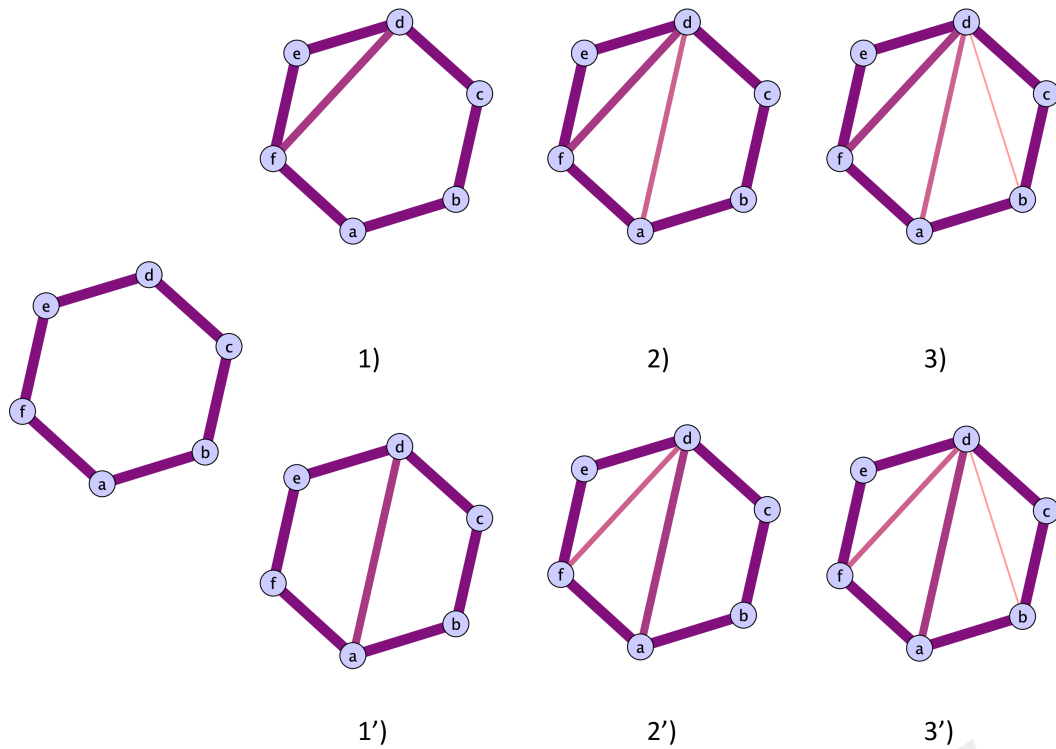


Figure 4. Illustration of the two possible routes a cycles can close. **Top route:** The cycles closes with the addition of triangles. The cycles representative will be the original cycles $\langle abcdef \rangle$, irrespectively of the life time of the sub cycles that are partially closed. **Bottom route:** The original cycle is split into smaller cycles that are eventually closed by the mechanism illustrated in the top route. The two cycles that will be represented in the original cycle $\langle abcdef \rangle$ and the subcycle $\langle abcd \rangle$, as the cycle $\langle adef \rangle$ can be obtained as a linear combination of the first two

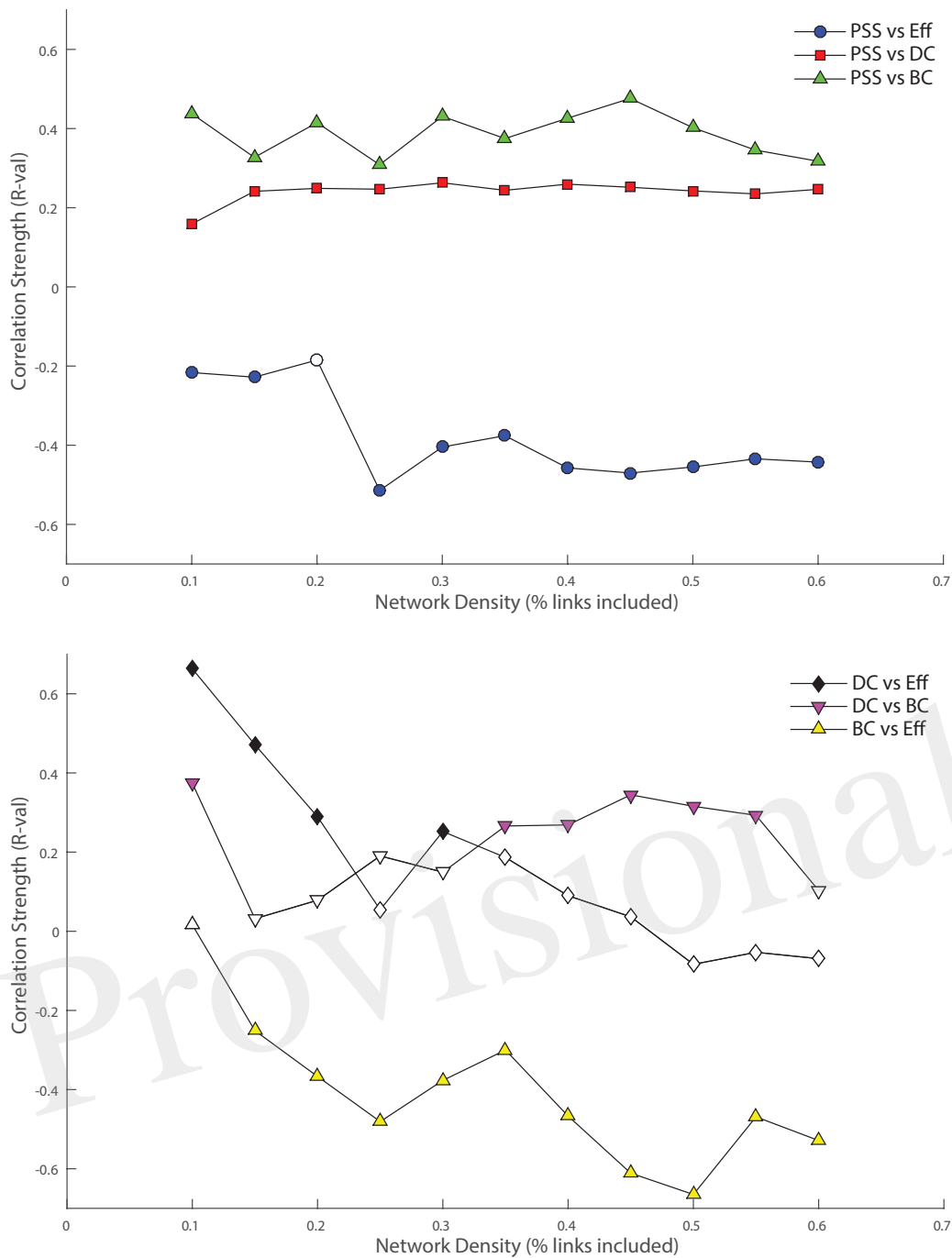


Figure 5. Top: Relationship between nodal persistence scaffold strength (*PSS*) and standard topological centrality measures. At each threshold under study, the value of the bivariate correlation coefficient (*R*) between *PSS* and each of: degree-centrality (*DC*), betweenness-centrality (*BC*) and local efficiency (*Eff*) is plotted. **Bottom.** Relationship between standard topological measures. The same procedure as above is repeated for correlations between: *DC* vs *BC*, *DC* vs *Eff*, and *BC* vs *Eff* as control conditions. **Filled shapes** indicate the presence of a **statistically significant** correlation between the two variables ($p < 0.05$).

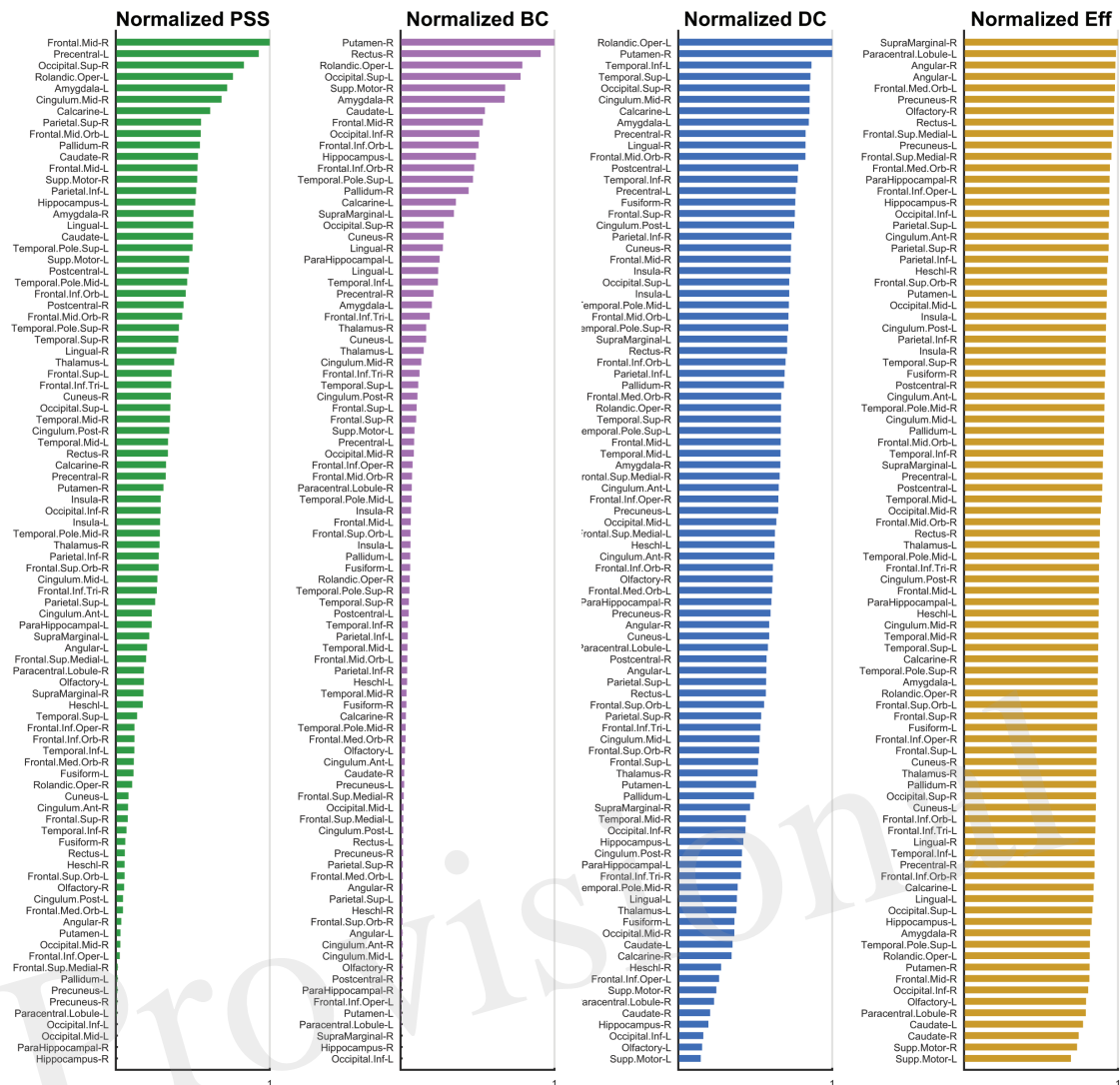


Figure 6. Normalized Metric Values. The normalized nodal values are displayed for each graph measure under study. The values for *PSS*, *BC*, *DC* and *Eff* are respectively depicted from left to right. While computation of the *PSS* does not require *ad hoc* thresholding, the *BC*, *DC* and *Eff* metrics are threshold-dependent and nodal metric values have thus been integrated over the threshold range under study to generate a single value for each node. The analysis used is described in detail section 3.2

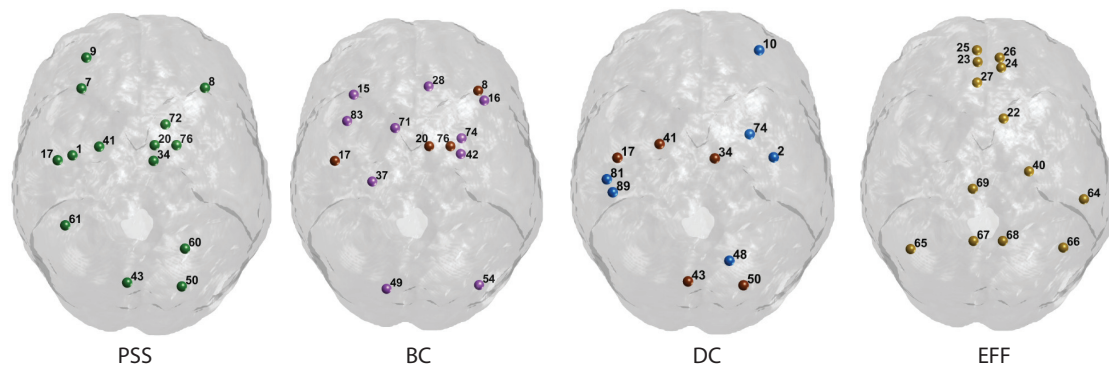


Figure 7. Graphical Display of the Highest-Ranking Nodes. Functional hubs identified on the *PSS* measure and three standard topological centrality metrics (*BC*, *DC*, *Eff*). Hubs on each measure are defined as having a value >1 S.D. of the mean of their respective distribution. Nodes overlapping with the *PSS* hubs are shown in brown. The corresponding AAL labels for each numerical index are included in supplementary figure S2.

Provisional